Nano Energy 144 (2025) 111389

Contents lists available at ScienceDirect

Nano Energy

journal homepage: www.elsevier.com/locate/nanoen

# Modular contact-electro-chemistry based on dielectrics with work function-tunable metal coatings

Jiajin Liu [a,b,1], Zhe Yang [a,b,1], Shaoxin Li [a,b,1], Han Qian [a,b], Ting Gan [a], Ning Wu [a,b], Zhong Lin Wang [a,c], Di Wei [a,d,*]

[a] Beijing Institute of Nanoenergy and Nanosystems, Chinese Academy of Sciences, Beijing 101400, PR China
[b] School of Nanoscience and Engineering, University of Chinese Academy of Sciences, Beijing 100049, PR China
[c] Georgia Institute of Technology, Atlanta, GA 30332-0245, United States
[d] Centre for Photonic Devices and Sensors, University of Cambridge, 9 JJ Thomson Avenue, Cambridge CB3 0FA, UK

ARTICLE INFO

*Keywords:*
Contact electrification
Contact-electro-chemistry
Radicals
Electronegativity
Modular reaction design

ABSTRACT

Catalysis is essential for energy conversion, environmental remediation, and industrial processes, with growing interest in non-noble metal and even non-metal systems. Contact-Electro-Chemistry (CE-Chemistry), driven by contact electrification (CE), offers a promising yet underexplored catalysis route with challenges in reaction efficiency. Here, we introduce a modular strategy using dielectric polymer/multilayer metal materials to optimize interfacial electron transfer and enhance reaction efficiency. Utilizing the synergistic effects of metal electronegativity, work function, and conductivity, the fluorinated ethylene propylene (FEP)/Cr/Cu film achieved a methyl orange degradation rate (0.1 mg/L·h·cm$^2$) at least 4 times higher than previous studies (0.0091–0.0249 mg/L·h·cm$^2$). The work function of the metal surface, determining reaction performance, can be regulated by CE through material electronegativity and hierarchical design. The outermost metal layer's conductivity was also shown to directly enhance reaction efficiency. Additionally, methanol-to-formaldehyde conversion via triboelectric charge-induced CE-Chemistry was nearly twice as efficient as with pristine FEP. This approach presents a novel paradigm for modular reaction design, enhancing CE-Chemistry efficiency while also enabling its synergistic integration with traditional catalysis to further improve catalytic performance. It expands the applicability of CE-Chemistry and opens new avenues in catalysis, advancing efficient, eco-friendly, and economically viable chemical reactions with tailorable kinetics for diverse applications.

## 1. Introduction

Catalysis is fundamental to a wide range of industrial processes, enabling efficient chemical reactions that reduce energy consumption and improve reaction selectivity [1]. It is a cornerstone technology in energy conversion, environmental remediation, and the fine chemical industry, where it lowers activation energies, accelerates reaction rates, and enhances selectivity [2]. In energy applications, catalysts are indispensable for reactions in fuel cells [3], water electrolysis for hydrogen production [4], and metal-air batteries [5], all of which contribute to advancing sustainable energy solutions. Similarly, in environmental applications, catalysts are essential for pollutant degradation, resource recycling, and improving ecological quality [6]. In traditional catalytic systems, noble metals such as platinum (Pt) [7], palladium (Pd) [8], iridium oxide ($IrO_2$)[9], and ruthenium oxide ($RuO_2$) [10] have been the materials of choice for key reactions, including the oxygen reduction reaction (ORR) and water oxidation reaction (WOR). These reactions are vital for clean energy systems like fuel cells and hydrogen production via electrolysis. The high catalytic activity and excellent selectivity of noble metals make them highly effective in these reactions [11]. However, their scarcity, high cost, limited recyclability, and susceptibility to deactivation during extended use pose significant challenges, particularly as global demand for low-carbon energy increases [12]. These drawbacks have driven the search for alternatives, shifting the focus toward non-noble metal catalysis and, more recently, to non-metallic solutions [13]. Although non-noble metals are more abundant and cost-effective, they still face issues such as lower intrinsic activity, reduced stability under harsh

* Corresponding author at: Beijing Institute of Nanoenergy and Nanosystems, Chinese Academy of Sciences, Beijing 101400, PR China.
*E-mail address:* weidi@binn.cas.cn (D. Wei).
[1] These authors contributed equally: Jiajin Liu, Zhe Yang, Shaoxin Li

https://doi.org/10.1016/j.nanoen.2025.111389
Received 3 July 2025; Received in revised form 10 August 2025; Accepted 12 August 2025
Available online 13 August 2025

conditions, and greater susceptibility to deactivation [14]. These limitations have spurred the search for non-metallic catalysis, such as carbon-based materials, capable of mimicking the active sites and functionalities of metals [15]. A promising approach in this emerging field involves combining non-noble metals with carbon substrates like graphene [16], enhancing catalytic performance while reducing dependence on costly and scarce metals. The growing trend in catalysis research is towards metal-free solutions, with non-metal catalysis emerging as a promising alternative [17]. This shift has the potential to transform energy and environmental catalysis, driving the development of more sustainable, efficient, and economically viable catalytic solutions.

In recent years, Contact-Electro-Catalysis (CEC) [18], based on the contact electrification (CE) phenomenon [19], has emerged as a new approach to drive chemical reactions, offering new avenues for the development of non-noble metal catalysis. Unlike traditional electrocatalysis, CEC drives reactions such as the ORR and WOR by utilizing triboelectric charge [20], i.e., charge transfer at the dielectric solid-liquid interface to generate reactive oxygen species (ROS) and accumulation of electrons on the dielectric surface [21], without relying on external electric bias or conductive electrodes. This mechanism overcomes the limitations of conventional electrocatalysis, expanding the catalytic surface area and enhancing reaction efficiency [22,23]. Unlike photocatalysis, that requires light irradiation, CEC operates effectively without light, using mechanical activation (e.g., ball milling [24], ultrasonic treatment [18], shake [25]) while maintaining chemoselectivity. This versatile energy input broadens its applicability in scenarios demanding controlled reaction pathways, even in dark environments. As a result, CEC has garnered significant interest for energy conversion and environmental protection, particularly for systems based on non-noble metals. CEC has been extensively utilized in diverse applications to drive reactions in aqueous [25] or nonaqueous [26] media, including the degradation of methyl orange (MO) [24], the cost-effective synthesis of hydrogen peroxide [27], mild luminol luminescence [28], and the sustainable recovery of metals from spent lithium-ion batteries [29]. Moreover, B. A. Grzybowski and co-workers pioneered the mechanistic understanding of CE phenomena at the microscopic level [25]. Based on this, our group has advanced this field by broadening the applicability of CEC to a wide array of chemical transformations and pioneering the concept of Contact-Electro-Chemistry (CE-Chemistry) [30]. However, despite its promising potential, CE-Chemistry faces several challenges in practical applications. One major issue is the effective regulation of electron transfer during the CE process. In aqueous systems, the formation of the electrical double layer (EDL) at the dielectric solid-liquid interface significantly hinders electron transfer, reducing the overall efficiency of the reaction [18,24,26]. Despite advances in enhancing charge transfer efficiency through strategies such as transitioning from aqueous to non-aqueous systems [26] and coating dielectrics with metals to modulate work functions [31], these approaches are still constrained by their reaction efficiency. Moreover, the interaction between different metals in CE-Chemistry systems, particularly in terms of work function adjustments, remains unclear and complicates the optimization of electron transfer [31]. Therefore, a key challenge moving forward is to enhance electron transfer efficiency in CE-Chemistry, particularly in aqueous environments, and to explore strategies that break through the existing limitations for more efficient and broadly applicable CE-Chemistry systems.

To address these challenges, this paper proposed a controllable modular design strategy that replaced traditional dielectrics in CE-Chemistry with a polymer/multilayer metal material. By utilizing CE effect between metals of varying electronegativity, the work function of the outermost metal could be regulated and the electron transfer efficiency can be optimized. Specifically, fluorinated ethylene propylene (FEP) was used as a substrate, and a series of FEP/multilayer metal materials were prepared using magnetron sputtering technology, with copper (Cu), chromium (Cr), and indium tin oxide (ITO) as functional metal layers. The CE effect induced by cavitation bubbles generated by ultrasound was studied to investigate the impact of metal electronegativity and conductivity on the efficiency of CE-Chemistry. For instance, in the degradation of MO, FEP/Cr/Cu material demonstrated a remarkable enhancement in reaction efficiency, achieving a degradation ratio of 79.05 % within 4 h, nearly threefold higher than that of pristine FEP (30.75 %) and surpassing the performance of monolayer metal FEP/Cu (52.45 %). Conversely, the MO degradation ratio for FEP/Cu/Cr was only 35.55 % over the same period, falling below that of monolayer metal FEP/Cr (44.45 %). This disparity arose from differences in electronegativity between the metals, facilitating electron transfer from the low electronegative metal (for example Cr, 1.66 based on Pauling electronegativity scale) to the high electronegative counterpart (for example Cu, 1.90) [32]. Moreover, compared to existing CE-Chemistry studies, the MO degradation efficiency achieved using the FEP/Cr/Cu film exceeds previous reports by more than 4 times. This approach modulated the electron escape capacity of surface metals, directing the reaction pathways of ORR and WOR and influencing ROS generation [33]. Additionally, the role of the outermost metal layer's conductivity was validated through variations in ITO thickness, demonstrating a clear positive correlation with electron transfer efficiency. Moreover, for the first time, the methanol-to-formaldehyde conversion was successfully achieved using the FEP/Cr/Cu film via triboelectric charge-induced CE-Chemistry, demonstrating nearly twice the reaction efficiency compared to the pristine FEP film under identical conditions. The proposed polymer/multilayer metal material not only enhanced the efficiency of CE-Chemistry but also leveraged the synergistic effects of metal electronegativity, work function, conductivity, and the CE performance of the underlying polymer. This strategy facilitated modular and simplified dielectric-based materials preparation, offering a novel pathway for controlling reaction kinetics in future chemical processes. While challenges remained, this method presented significant potential for reducing production costs and environmental impact, aligning seamlessly with the principles of green chemistry and sustainable development goals.

## 2. Results

### 2.1. Proposed mechanism of FEP/multilayer metal material

CE-Chemistry has advanced significantly since its inception, evolving from simple dielectric polymer materials to polymer/metal material with increasingly refined reaction mechanisms and improved efficiencies [18,31]. However, further enhancement of reaction efficiency remains a formidable challenge that limits broader applicability. In this study, we proposed a polymer/multilayer metal material structure. Metals with varying electronegativities (Cu, Cr) and a polymer material (FEP) exhibiting superior CE properties were selected. Polymer/multilayer metal material used in CE-Chemistry were prepared by depositing metals onto the FEP surface using magnetron sputtering under an argon atmosphere, followed by ultrasonic bath-assisted reactions. The sputtering rates were determined to be 4.8 nm/min for Cu and 5 nm/min for Cr, with thickness measured by a step profiler (Figure S1). The single-layer metal thickness was standardized at 500 nm, while double-layer materials were designed with each layer set to 250 nm, maintaining a consistent total metal thickness. Scanning electron microscopy (SEM) and energy-dispersive X-ray spectroscopy (EDX) elemental mapping (Figure S2) revealed the surface morphology and elemental distribution of FEP and the metal coatings. Cross-sectional imaging of FEP/Cr/Cu (Figure S3) displayed distinct color transitions, confirming the deposition of thin metal films on the FEP substrate. Atomic force microscopy (AFM) analysis of the surface topography confirmed the high uniformity of the sputtered coating (Figure S4). X-ray photoelectron spectroscopy (XPS) survey scans of FEP/Cu and FEP/Cr (Figure S5) confirm the chemical integrity of the magnetron-sputtered films, showing predominant photoelectron signals

corresponding to Cu 2p, O 1 s, and C 1 s for FEP/Cu, and Cr 2p, O 1 s, and C 1 s for FEP/Cr [34]. The absence of extraneous metallic species (below the 0.01 at% detection limit) confirms a contamination-free sputtering process from the Cu target and rules out unintended intermetallic diffusion during deposition. The XPS survey scan of FEP/Cr/Cu (Figure S6) further validates the chemical integrity of the magnetron-sputtered films, showing predominant photoelectron signals corresponding to Cu 2p, O 1 s, and C 1 s [35]. These findings collectively indicate the absence of direct interlayer diffusion between the metal films.

Fig. 1a illustrated the fundamental CE-Chemistry mechanism using pristine FEP. Cavitation bubbles generated during ultrasonication induced CE between FEP and water, resulting in electron transfer and hydroxyl radical (·OH) formation. Electrons on the FEP surface were subsequently captured by oxygen, forming superoxide radicals ($\cdot O_2^-$) [36,37]. Although these two radicals collectively drove the reaction, the efficiency remained relatively low. The mechanism of CE was elucidated by the electron-cloud-potential-well model [19]. As depicted in Figure S7, atoms are attracted when they exceed the equilibrium distance, but when they approach, their electron clouds overlap, causing repulsion. This overlap promotes electron transfer, highlighting the crucial role of the potential barrier in governing the CE process. Fig. 1b showed the introduction of a single-layer metal coating via magnetron sputtering [31]. The strong electric field induced by the negative charge on FEP during CE caused internal electrons in the metal to migrate outward, generating an induced electric field that balanced the electric field on the FEP side. This simultaneously lowers the metal's work function, facilitating electron escape from metal surface to generate more ROS for improving reaction efficiency. Fig. 1c presented the structure and mechanism of the polymer/multilayer metal material. It was reported that the difference in metal electronegativity would drive electron transfer from the low electronegative metal (Cr) to the high electronegative one (Cu) [38]. This process increased the electron density on the high electronegative metal, lowering the work function of high electronegative metal and making electron escape easier, while the electron density decreased on the low electronegative metal, increasing the work function of low electronegative metal and hindering electron escape. Fig. 1d presented the calculated work functions of the outermost metal layers in different polymer/metal layer structures, as derived from ultraviolet photoelectron spectroscopy (UPS) measurements (Figure S8). Compared to FEP/Cu (electronegativity of 1.90), the work function of Cu in FEP/Cr/Cu decreased by 0.85 eV, while the work function of Cr in FEP/Cu/Cr increased by 0.81 eV compared to FEP/Cr (electronegativity of 1.66). This indicated that differences in metal electronegativity can modulate the work function of the outermost metal layer, controlling electron escape.

As demonstrated by the degradation of MO, a 20 mm × 50 mm FEP/multilayer metal material was introduced into a 10 ml solution of MO with a concentration of 5 ppm, and subsequently subjected to ultrasonic treatment within a thermostatically controlled water bath, as shown in Fig. 1e. Following a 4-hour ultrasonication period, CE-Chemistry employing pristine FEP resulted in a mere 30.75 % degradation ratio (The degradation ratio refers to the percentage of MO decomposed over a specified period under defined conditions) of MO. When coated with a singular metallic layer, the MO degradation ratio escalated to 52.45 % for FEP/Cu and 44.75 % for FEP/Cr, indicative of an augmented reaction efficiency. Notably, FEP/Cr/Cu achieved an impressive MO degradation ratio of 79.05 % after 4 h (the color change of MO with ultrasonication was shown in Figure S9), surpassing the best performance of FEP coated with singular metallic layer, i.e., FEP/Cu (52.45 %). In contrast, FEP/Cu/Cr achieved only 35.55 %, showing even lower efficiency than FEP/Cr. Critically, the stark contrast in catalytic performance between FEP/Cr/Cu (79.05 %) and FEP/Cu/Cr (35.55 %), despite identical metal thicknesses and processing conditions, provides definitive evidence for an electronegativity-driven electron transfer mechanism. This systematic variation decisively rules out Schottky barrier effects as the dominant factor. Furthermore, to systematically investigate the influence of the inner metal's electronegativity on reaction efficiency, the outer metal layer in the multilayer composite was held constant. When gold (Au, electronegativity of 1.66), possessing a higher electronegativity, was employed as the inner metal layer, the resulting FEP/Au/Cu exhibited a MO degradation efficiency of merely 40.35 % after 4 h (Figure S10). This degradation efficiency falls significantly below the 79.05 % benchmark of FEP/Cr/Cu, providing

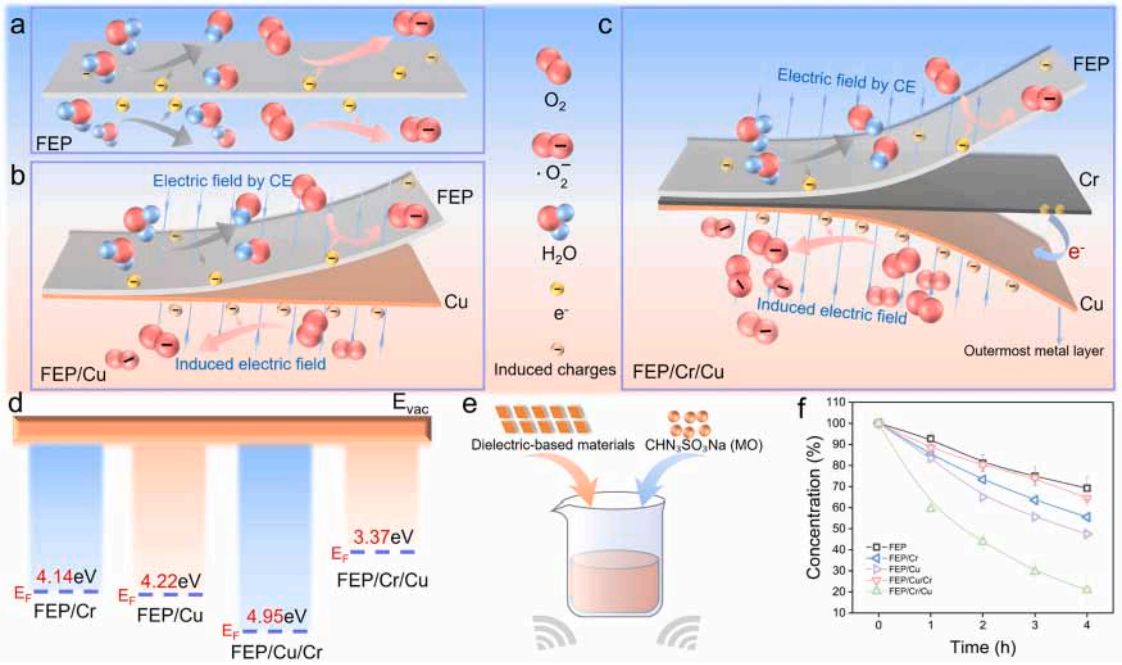


**Fig. 1.** Proposed Mechanism of FEP/Multilayer Metal Material. The mechanism of CE-Chemistry, a) pristine FEP, b) FEP/metal material, c) FEP/multilayer metal material. d) Measured work function of the Cr layer of FEP/Cr and FEP/Cu/Cr, the Cu layer of FEP/Cu and FEP/Cr/Cu. e) Schematic of the experimental setup and protocol. f) The ratios of MO degradation with different dielectric-based materials.

conclusive evidence for an electronegativity-driven electron transfer mechanism. Furthermore, to verify the advantage of symmetric metal layers, we prepared FEP/Cr/Cu materials with metal thicknesses of Cr 100 nm and Cu 400 nm. It was found that the degradation rate of MO after 4 h for this asymmetric structure material was only 53.8 % (Figure S11), lower than that of the symmetric structure (79.05 %). Therefore, symmetric FEP/Cr/Cu was selected for subsequent experiments. To conclusively demonstrate the critical role of the FEP-mediated interface, control experiments were conducted using standalone Cr/Cu metallic films with equivalent surface areas (Figure S12). Strikingly, the pure metallic system without FEP support exhibited drastically reduced MO degradation efficiency, achieving merely 10.35 % removal after 4 h. This pronounced performance gap unequivocally affirms that it is the polymer-metal interfacial synergy, rather than the metallic constituents alone, that fundamentally governs the chemical activation mechanism. This suggested that the electronegativity of intermediate metal layer affects electron escape from the outermost metal layer, thereby modulating ROS generation and regulating of chemical reaction efficiency.

### 2.2. *Impact of metal layer configuration on CE-Chemistry*

The electron transfer mechanism between multilayered metals and the effect of the outermost metal on the reaction were investigated. To demonstrate the influence of electronegativity on electron transfer between metals, the electronic structure of specific elements was analyzed using XPS. In XPS, a decrease in binding energy indicates that the target atom resides in an environment of higher electron density [39]. The direction of charge transfer can be characterized by shifts in element-specific binding energies: an increase signifies electron loss, while a decrease corresponds to electron gain [38,39]. In XPS analysis, the Cu 2p1/2 and 2p3/2 peaks, arising from spin-orbit splitting of the 2p orbital, serve as critical indicators to probe electron density changes of

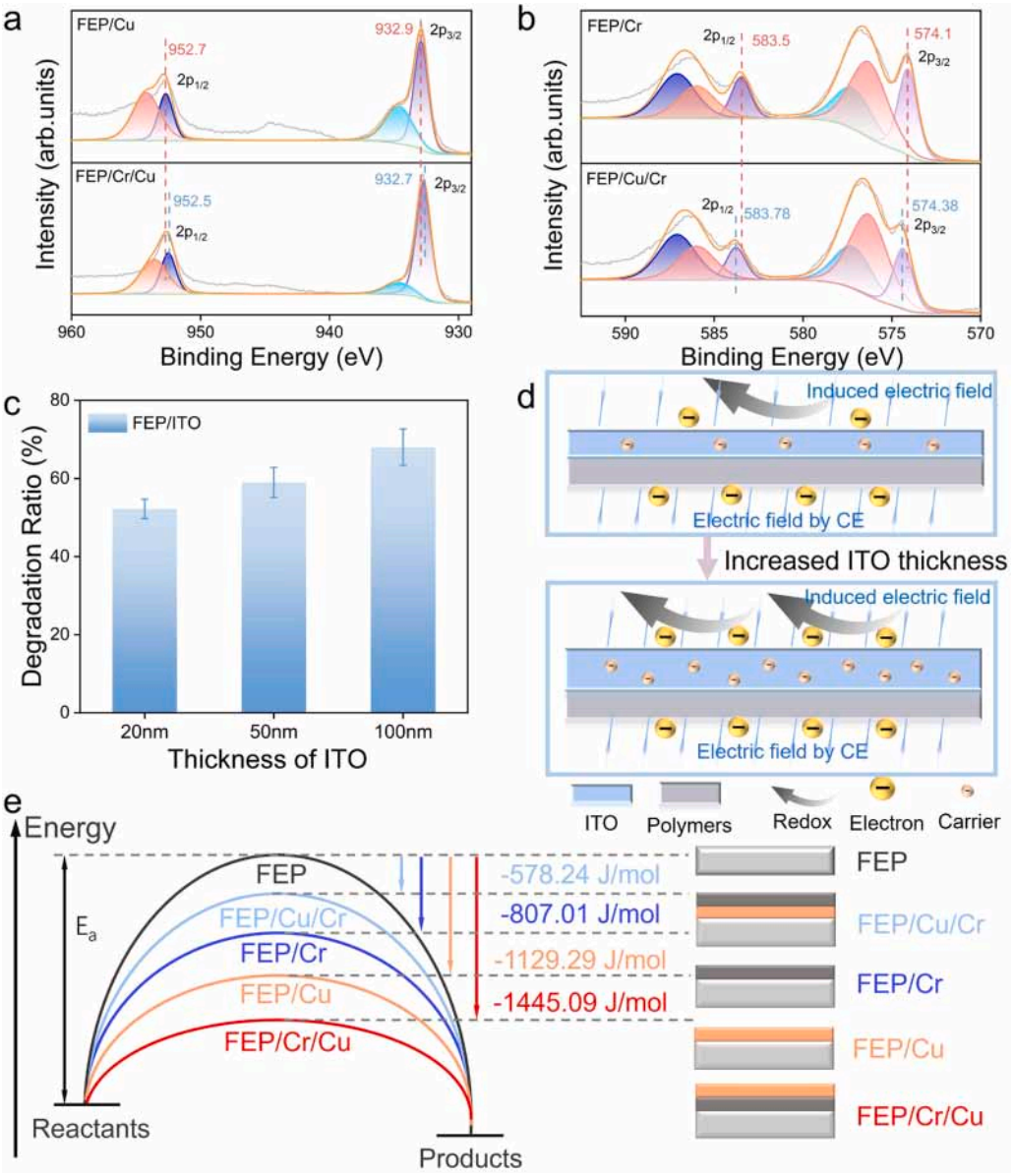


**Fig. 2.** Impact of Metal Layer Configuration on CE-Chemistry. a) Variations in the 2p binding energy of Cu in FEP/Cu and FEP/Cr/Cu. b) Variations in the 2p binding energy of Cr in FEP/Cr and FEP/Cu/Cr. c) Reaction activity of FEP/ITO as a function of ITO thickness. d) Schematic illustration of the effect of metal terminal material conductivity on the driving chemical reaction performance of FEP/ITO, indicating that increased ITO thickness enhances charge carrier density and facilitates electron transport. e) Effect of metal layer configuration on the activation energy for $\cdot O_2^-$ generation. The schematic on the right depicts different dielectric-based materials structures.

Cu through their binding energy shifts[40]. Similarly, the Cr 2p1/2 and 2p3/2 peaks reflect Cr's electronic environment[41]. The electronic states of FEP/Cu, FEP/Cr/Cu, FEP/Cu/Cr, and FEP/Cr were measured. For FEP/multilayer metal material with Cu as the outermost layer, a shift in binding energy was observed: from 932.9 eV (FEP/Cu) to 932.7 eV (FEP/Cr/Cu) for 2p3/2 and from 952.7 eV (FEP/Cu) to 932.5 eV (FEP/Cr/Cu) for $2p_{1/2}$ (Fig. 2a) Experimental results showed a 200 meV decrease in the 2p binding energy after introducing Cr, a metal with lower electronegativity. This confirmed that electron transferred from Cr to Cu, increasing the electron density of Cu and reducing the work function of Cu [38]. For FEP/multilayer metal material with Cr as the outermost layer, a shift in binding energy was observed: from 574.1 eV (FEP/Cr) to 574.38 eV (FEP/Cu/Cr) for $2p_{3/2}$ and from 583.5 eV (FEP/Cr) to 583.78 eV (FEP/Cu/Cr) for $2p_{1/2}$ (Fig. 2b). An increase of 280 meV in the 2p binding energy after introducing Cu, a high electronegative metal, further confirmed electron transfer from Cr to Cu. This transfer reduced the electron density of Cr, raising the work function of Cr. Furthermore, DFT simulations were employed to investigate the direction of electron transfer between metals, and the results aligned with XPS analysis, confirming that electron transfers from Cr to Cu (Figure S13). This finding further highlighted the influence of electronegativity on electron transfer dynamics. The modulation of metal work functions through CE driven by differences in metal electronegativity, enabled precise control over radical generation and facilitated the fine-tuning of chemical reactions.

Additionally, the resistivity of the outermost metal layer influenced reaction efficiency in CE-Chemistry, leading to variations in MO degradation ratios observed for FEP/Cu (52.45 %) and FEP/Cr (44.75 %). To explore this, FEP/ITO samples with varying coating thicknesses were tested, and their resistivity was presented in Figure S14. As shown in Fig. 2c, increasing the ITO thickness reduced resistivity and elevated the MO degradation ratio from 52.2 % to 68 %. This observation indicated that materials with higher electrical conductivity enhance electron escape, thereby promoting ROS formation and improving reaction efficiency (Fig. 2d). The change in activation energy, derived from the Arrhenius equation [42], was used to quantify the contribution of the metal layers (Figure S15). As shown in Fig. 2e, compared to pristine FEP, the activation energy for $\cdot O_2^-$ generation from molecular oxygen in CE-Chemistry decreased to $-1445.09\ J{\cdot}mol^{-1}$ with FEP/Cr/Cu and to $-1129.29\ J{\cdot}mol^{-1}$ with FEP/Cu. This enhancement demonstrated that more electrons can be induced on the metallic surface, facilitating electron exchange. Furthermore, electron transfer between metals increased the electron density on the outermost metal surface, making electron escape more efficient.

### 2.3. Study on ROS generation in CE-Chemistry by FEP/multilayer metal material

To measure the charges generated by the CE between FEP and water, a triboelectric nanogenerator (TENG) operating in a contact-separation mode was designed [43,44]. The CE mechanism of the TENG was illustrated in Figure S16. Upon contact with water, an accumulation of approximately 1.27 nC of negative charges was observed on the FEP surface (Fig. 3a), with the experimental setup depicted in Fig. 3b. Consequently, the negative triboelectric charges via CE on the FEP surface induced a corresponding electric field, prompting the migration of electrons in the outer metallic layer outward, thereby facilitating the generation of ROS [31]. In CE-Chemistry, two representative ROS reactions were commonly observed: the WOR, where electrons were extracted from water molecules to produce ·OH, and the ORR, where electrons were donated to oxygen to generate $\cdot O_2^-$. Here, FEP, FEP/Cr, FEP/Cu, FEP/Cu/Cr, and FEP/Cr/Cu were acted as dielectric-based

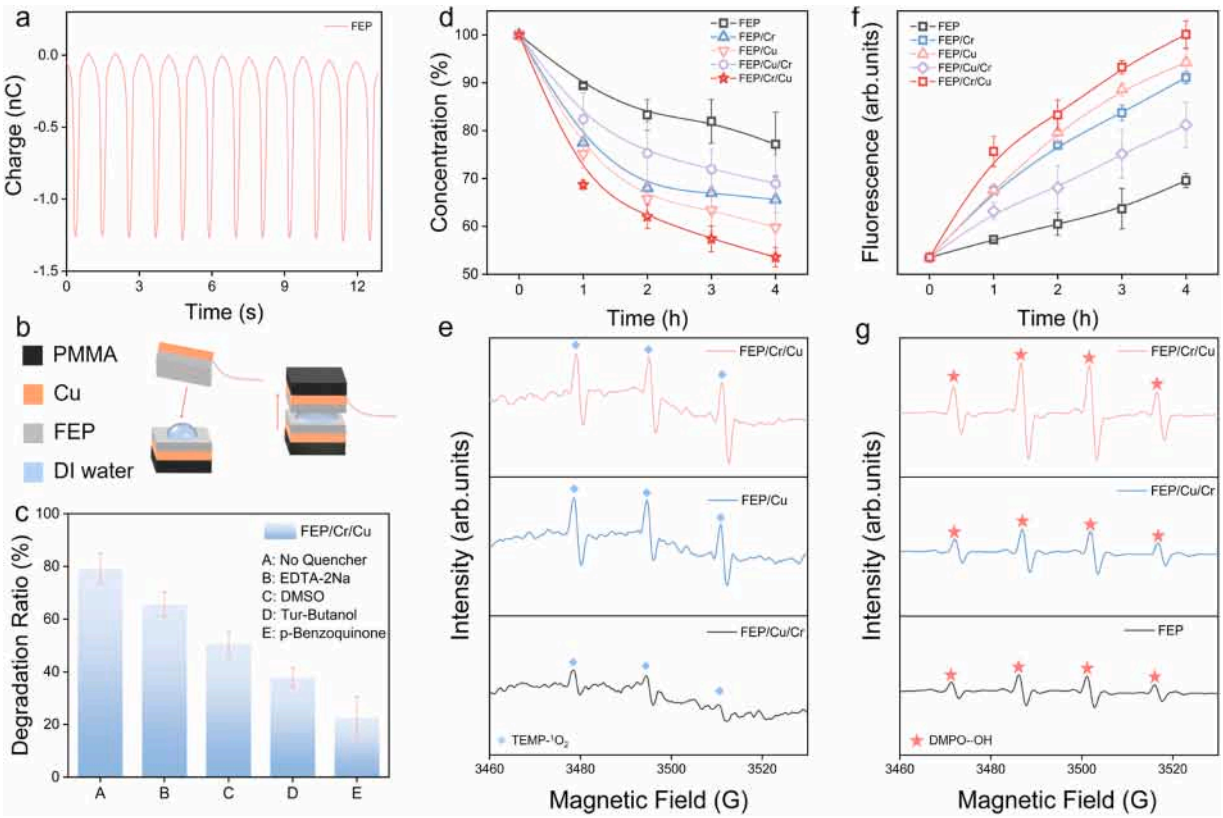


**Fig. 3.** FEP/Multilayer Metal Material Regulation of ROS. a) Triboelectric charging of the FEP film upon contact with water. b) The experimental setup of TENG. c) Evolution of MO relative concentration in the presence of FEP/Cr/Cu under various radical scavengers (each at a final concentration of 1 mM). The lower section illustrates a schematic of the TENG mechanism. d) Detection of ·O2- using NBT. e) Detection of 1O2 through EPR using TEMP to form a triplet peak. f) Detection of ·OH using THA. g) Detection of ·OH through EPR using DMPO to form a quartet peak.

materials in CE-Chemistry to elucidate their distinct roles in facilitating ROS generation. To verify the impact of different radicals on the reaction, a series of radical scavengers (1 mM) were added to a sample solution containing 5 ppm MO. Ethylenediaminetetraacetic acid disodium salt (EDTA-2Na), dimethyl sulfoxide (DMSO), tert-butanol, and p-benzoquinone were used as scavengers for protons, electrons, ·OH, and $\cdot O_2^-$, respectively [18]. As shown in Fig. 3c, the addition of these scavengers significantly reduced the reaction rate, indicating the crucial roles of ·OH and $\cdot O_2^-$ in the process. When $\cdot O_2^-$ were quenched, the MO degradation ratio after 4 h of ultrasonication dropped to 22.5 %. When ·OH were quenched, the degradation ratio decreased to 37.9 %. These results emphasized the importance of these radicals in the reaction system, demonstrating that precise control over the production of ·OH and $\cdot O_2^-$ could effectively regulate chemical reactions.

To provide a more direct demonstration of the reaction effects of different FEP/multilayer metal material on the generation of $\cdot O_2^-$ and ·OH, the following experiments were conducted. The generation of $\cdot O_2^-$ (ORR reaction) was evaluated using a UV-Vis spectrophotometer by measuring the absorbance of nitrotetrazolium blue chloride (NBT) after reacting with $\cdot O_2^-$ (Figure S17). As shown in Fig. 3d, NBT exhibited the highest reduction rate in the presence of FEP/Cr/Cu, which was 2.03 times higher than that of FEP and exceeded that of FEP/Cu. However, the reduction rate for FEP/Cu/Cr was lower than that of FEP/Cr. Therefore, regulating the outermost metal layer with a high charge density through differences in electronegativity was a key factor in enhancing chemical reaction efficiency by promoting the generation of $\cdot O_2^-$. This phenomenon was further corroborated by electron paramagnetic resonance (EPR) spectroscopy (Fig. 3e). Singlet oxygen ($^1O_2$), an oxidative product of $\cdot O_2^-$ [45], was significantly promoted by FEP/Cu, indicating enhanced ORR. Moreover, FEP/Cr/Cu further promoted $\cdot O_2^-$ generation, underscoring the role of electron transfer between metals in facilitating the ORR. Conversely, FEP/Cu/Cr inhibited $\cdot O_2^-$ generation, emphasizing the regulatory effect of electron transfer on the ORR. In addition, the generation of ·OH was evaluated using a fluorescence spectrophotometer by detecting fluorescence resulting from the reaction between terephthalic acid (THA) and ·OH (Figure S18). As shown in Fig. 3f, FEP/Cr/Cu exhibited the highest fluorescence intensity, which was 1.87 times higher than that of FEP and exceeded that of FEP/Cu. However, the fluorescence intensity of FEP/-Cu/Cr was lower than that of FEP/Cr. Fig. 3g presented the characteristic DMPO-·OH quadruple peaks, which followed the same trend as the THA fluorescence results.

In summary, the ROS generation efficiency of the five dielectric-based materials followed the reaction activity trend: FEP/Cr/Cu > FEP/Cu > FEP/Cr > FEP/Cu/Cr > FEP. Therefore, we proposed that electron transfer between water molecules and FEP during CE generated an electric field. This electric field induced electron flow within the FEP/multilayer metal material. Additionally, electron transfer between multilayer metals, driven by differences in metal electronegativity, either promoted or suppressed electron flow, thereby modulating the reaction. In FEP/Cr/Cu, the highest ORR efficiency was achieved, likely due to electron accumulation on the Cu surface facilitated by electron transfer from Cr. This promoted electron transfer to oxygen molecules, enhancing $\cdot O_2^-$ generation. Furthermore, the CE-derived electric field facilitated water molecule dissociation, accelerating ·OH generation. As a result, both ORR and WOR exhibited excellent performance, significantly enhancing ROS production. These experimental findings demonstrated that regulating chemical reactions through electron accumulation in polymer materials, electron escape in metal materials, and electron transfer between metals was a feasible strategy. Notably, the FEP/Cr/Cu composite film demonstrated exceptional operational stability, as evidenced by cyclic testing results (Figure S19). After 20 consecutive reaction cycles, the reaction system maintained > 93 % of its initial degradation efficiency, confirming remarkable structural integrity and resistance to deactivation under mechanical stress conditions.

### 2.4. Regulating the mechanism of FEP/ multilayer metal material

Fig. 4a illustrated the variation in the work function of the outermost metal, Cu, in the polymer/Cr/Cu sample under electric fields of varying intensities and directions. In a negative electric field generated by charges on the polymer surface, the Cu work function decreased from 3.58 eV to 3.44 eV as the field strength increases from 0 to 100,000 kV/m, indicating a reduced energy barrier for electron escape. In contrast, in a positive electric field, the work function increased with field strength, facilitating electron attraction from the environment and hindering escape. These simulations demonstrated that metal work functions could be precisely tuned by modulating the CE properties of the polymer, enabling controlled chemical reactions. Fig. 4b elucidated the driving chemical reaction mechanism of polymer/multilayer metal material in CE-Chemistry. On the FEP surface, ·OH and $\cdot O_2^-$ were generated via electron transfer driven by CE. Due to the high electron affinity of the abundant fluorine (F) elements on the FEP surface, the electron transfer rate for generating $\cdot O_2^-$ was relatively slow, leading to the continuous accumulation of negative charges on the FEP surface. This charge accumulation established an electric field in the surrounding space, maintaining a high electric field intensity on the FEP surface. The metal layer on the rear side of FEP was influenced by this electric field, causing electron accumulation on the outermost surface of the metal due to electrostatic induction. These surface electrons readily underwent electron exchange with oxygen, experiencing weaker constraints compared to those on the FEP surface Moreover, the high-intensity electric field generated by CE not only lowered the metal's work function, reducing the energy barrier to facilitate electron donation, but also polarized nearby water molecules, thereby accelerating the generation of ·OH. In multilayer metals, electron transfer occurred from the low electronegative metal (Cr) to the high electronegative metal (Cu) due to their difference in electronegativity. Taking FEP/Cr/Cu as an example, electrons transfer from Cr to Cu, increasing the charge density on the Cu surface, lowering its work function, and enhancing electron escape. This promoted the ORR, increasing the generation of $\cdot O_2^-$. Conversely, in the FEP/Cu/Cr configuration, electron transfer reduced the charge density on the Cr surface, raising its work function, inhibiting electron escape, and thus suppressing the ORR, resulting in reduced $\cdot O_2^-$ generation. Through the synergistic regulation of the electric field on the polymer surface and electron transfer between metals, the ORR reaction and the efficiency of CE-Chemistry could be effectively controlled. Previous studies on CE-Chemistry have been summarized, with a focus on methods such as thin-film modification to enhance reaction efficiency. These have been compared with the present work, as illustrated in Fig. 4c [31,46–48]. Compared to previous studies, the FEP/Cr/Cu film significantly increased the degradation efficiency of MO, achieving more than 4 times the efficiency of other works, with detailed data provided in Table S1. This further validated the ability of our approach to enhance or modulate reaction efficiency through the differences in electronegativity between metals.

Figure S20-S21 presented the morphological characterization and elemental mapping of FEP/Cr/Cu before and after CE-Chemistry. No significant morphological changes were observed through visual inspection and SEM analysis. Furthermore, elemental mapping using EDX confirmed that the composition of FEP/Cr/Cu remained unchanged. The X-ray diffraction (XRD) spectra in Figure S22 showed no shift in diffraction peak positions before and after the reaction. XPS was employed to analyze the chemical state changes of FEP/Cr/Cu before and after the reaction. The Cu 2p spectra, shown in Figure S23, revealed no changes in the binding energy of the original peaks or the appearance of new peaks after MO degradation. This further verified the chemical stability of FEP/Cr/Cu during the CE-Chemistry process.

### 2.5. Broad applications of CE-Chemistry

Building on the concept of modular reaction design with work

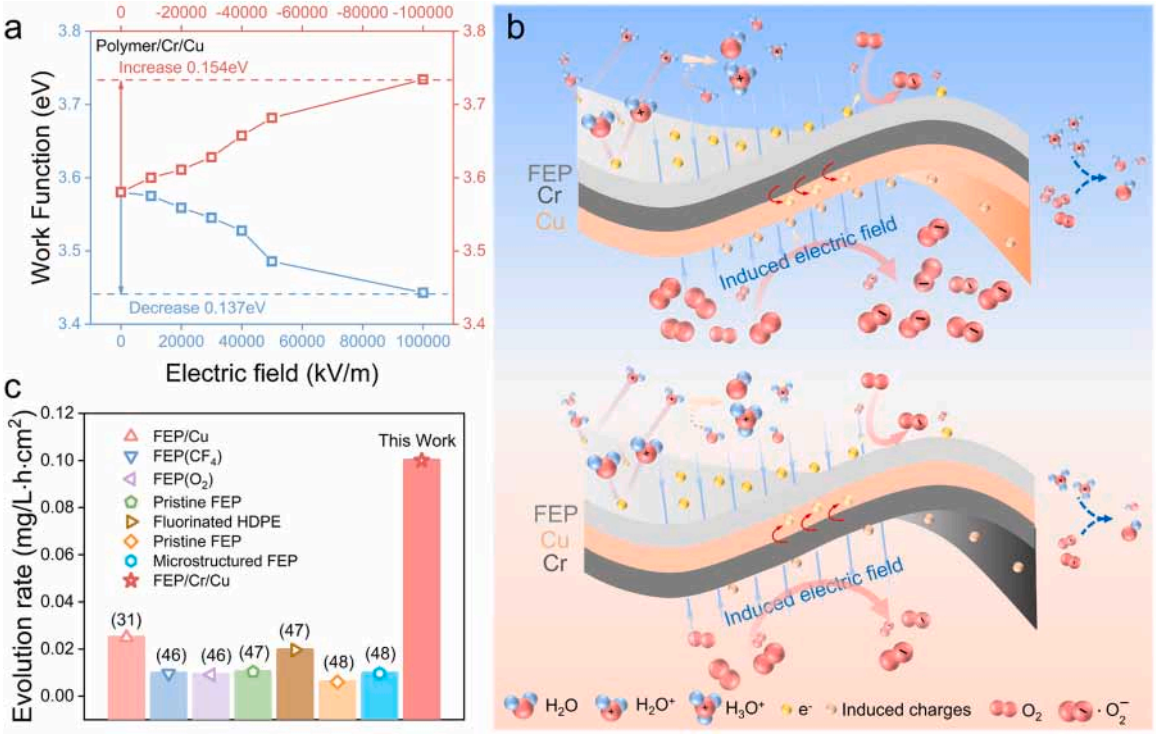


**Fig. 4.** The mechanism of CE-Chemistry in FEP/Multilayer Metal Material with different metal structures. a) Evolution of the Cu work function in FEP/Cr/Cu under different electric field conditions. b) Proposed mechanism for regulating CE efficiency in the presence of FEP/multilayer metal material (top: FEP/Cr/Cu, bottom: FEP/Cu/Cr). c) Degradation rate of MO compared to other methods of CE-Chemistry.

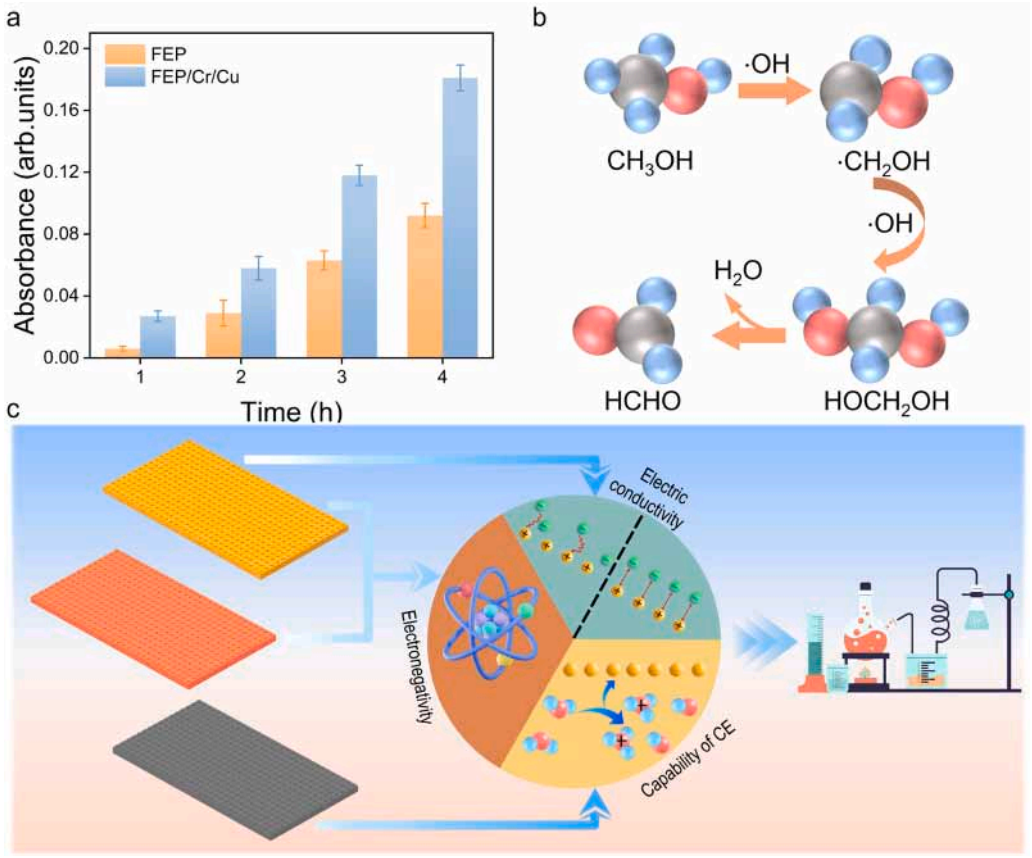


**Fig. 5.** Broad applications of CE-Chemistry. a) Detection of HCHO conversion via spectrophotometry using acetylacetone. b) Mechanism of $CH_3OH$ conversion to HCHO. c) Future prospects for CE-Chemistry.

function-tunable metal coatings, this study further explores the modulation of metal electronegativity in complex organic synthesis systems, underscoring its substantial potential for broad applications in driving chemical reactions. HCHO, a key platform molecule with an annual global production exceeding 30 million metric tons, serves as a critical precursor for urea-formaldehyde resins, engineering plastics, and functional coatings [49]. Furthermore, it serves as a critical intermediate in artificial carbon dioxide ($CO_2$) fixation pathway [50], where its production yield directly governs the efficiency of subsequent catalytic steps. Given its widespread industrial applications, improving the efficiency and sustainability of HCHO production is of paramount importance. Conventional thermal catalytic methods, typically utilizing high-temperature oxide catalysts like $V_2O_5/SiO_2$ at 600°C [51], suffer from significant drawbacks, including methanol over-oxidation to $CO_2$, catalyst deactivation due to thermal sintering, and high energy consumption [52]. Additionally, the high-temperature conditions necessitate expensive infrastructure and increase operational costs. Electrocatalytic HCHO synthesis [53], while operating under milder conditions than thermal methods, faces significant drawbacks, including the reliance on external electrical inputs, which limits achievable current densities and constrains catalytic efficiency. Additionally, the process often suffers from poor product selectivity due to competing side reactions and electrode over-potentials, further complicating scalability and economic viability. These challenges highlight the need for alternative approaches to improve energy efficiency and selectivity in HCHO production.

Here, we reported, for the first time, the efficient conversion of $CH_3OH$ to HCHO using CE-Chemistry, without noble metal catalysts, significantly reducing both energy consumption and operational costs. FEP films or FEP/Cr/Cu films (20 mm × 50 mm) were cut into smaller pieces (5 mm × 5 mm) and added to a 10 ml solution with a water-to-$CH_3OH$ ratio of 30:1, followed by ultrasonic treatment. It was also tested using HCHO and acetylacetone to produce a yellow compound with an absorbance at 412 nm (Figure S24) [54]. As shown in Fig. 5a, the addition of FEP/Cr/Cu resulted in a yield nearly twice as high as that of FEP alone, significantly enhancing the reaction rate. The mechanism of $CH_3OH$ oxidation to HCHO was illustrated in Fig. 5b. $CH_3OH$ reacted with ·OH to form the intermediate $\cdot CH_2OH$, which subsequently underwent oxidation to yield HCHO [55,56]. This aligned with the earlier experiment results of ·OH where FEP/Cr/Cu facilitated the generation of more ·OH, thereby accelerating $CH_3OH$-to-HCHO conversion. The integration of tunable work function metal coatings in CE-Chemistry further optimizes reaction efficiency and selectivity while mitigating over-oxidation. This approach represents a breakthrough in catalytic chemistry, overcoming the limitations of traditional methods and providing a more efficient, cost-effective, and environmentally friendly pathway for large-scale HCHO production.

Furthermore, by designing polymer/multilayer metal systems tailored to metal electronegativity, conductivity, and work function, we enable precise control over electron transfer dynamics and radical generation efficiency. This modular approach opens new pathways for fine-tuning reaction selectivity in CE-mediated chemistry, offering a sustainable platform for industrial chemical synthesis.

## 3. Discussion

Catalysis is pivotal for driving chemical reaction,energy conversion, environmental remediation, and industrial processes, with growing emphasis on cost-effective non-noble metal and even non-metal systems. CE-Chemistry, driven by triboelectric charge via CE at dielectric-liquid interfaces, holds great potential but faces efficiency challenges. Here, we present a modular strategy using dielectric polymer/multilayer metal materials to optimize interfacial electron transfer, markedly enhancing the efficiency of CE-Chemistry through the synergistic effects of metal electronegativity, work function, conductivity, and dielectric CE performance. The FEP/multilayer metal material developed harnesses both the electric field generated by triboelectric charges on FEP to drive chemical reactions and the electron transfer induced by electronegativity differences between metals to modulate reaction pathways. Compared to pristine FEP, both FEP/Cu and FEP/Cr enhanced ROS generation, improving reaction efficiency due to the electric field generated by CE between FEP and water, which lowered the metal work function and facilitated electron transfer. Notably, FEP/Cr/Cu outperformed FEP/Cu, achieving a 1.6-fold increase in MO degradation efficiency within 4 h and reducing the Cu work function by 0.85 eV. This improvement stemmed from intermetallic electron transfer, where electrons migrated from the less electronegative Cr (1.66) to the more electronegative Cu (1.90). XPS analysis confirmed this, showing a 200 meV shift in Cu binding energy for FEP/Cr/Cu compared to FEP/Cu. In contrast, FEP/Cu/Cr (35.55 %) displayed lower reaction efficiency than FEP/Cr (44.45 %), with an increased Cu work function (0.81 eV), underscoring the importance of intermetallic electron transfer. Furthermore, the methanol-to-formaldehyde conversion was successfully achieved for the first time using the FEP/Cr/Cu film via triboelectric charge-induced CE-Chemistry, demonstrating nearly twice the reaction efficiency compared to the pristine FEP film under identical conditions. This strategy enabled straightforward, modular reaction design based on various dielectric and metal materials, offering a novel approach to controlling reaction pathways and rates in chemical processes. Notably, the work function of metals in driving chemical reactions could be further tuned by CE. This insight suggests that combining traditional catalytic processes with our CE-Chemistry could synergistically enhance catalytic efficiency. The method holds significant promise for reducing production costs and environmental impacts, aligning with green chemistry principles and sustainable development goals.

### 3.1. Materials and methods

**Materials:** Fluorinated ethylene propylene (FEP) film were supplied by Dupont.

**Chemical reagents:** The methyl orange ($C_{14}H_{14}N3NaO_3S$, 98 %), p-benzoquinone ($C_6H_4O_2$, 99.5 %), p-phthalic acid ($C_8H_6O_4$, 99 %), nitrotetrazolium blue chloride (C40H30N10O6·2Cl, 98 %) methanol ($CH_4O$,99.5 %) were purchased from Macklin. Dimethyl sulfoxide (DMSO) was purchased from Shanghai Acmec Biochemical Technology Co., Ltd. Tert-butanol (98.0 %) was purchased from Sinopharm Chemical Reagent Co. Ltd. The 5,5-Dimethyl-1-pyrroline N-Oxide ($C_6H_{11}NO$), 2,2,6,6Tetramethyl-4-piperidone hydrochloride ($C_9H_{20}N$) were obtained from Dojindo.

### 3.2. Fabrication of FEP/multilayer metal materials

FEP/Multilayer Metal Composite Catalysts were prepared by magnetron sputtering (YuanRong Magnetron Coating Instrument, YNS-600). Cu and Cr nanoparticles were deposited on the surface of the precleaned polymer membranes by sputtering from the respective targets (purity, 99.99 %). The base pressure of the sputter chamber was kept below $10^{-8}$ Pa prior to sputtering. Ultrapure argon was then applied to provide a working pressure of $10^{-3}$ Pa to ensure elimination of possible contamination of the chamber. Subsequently, we turned on 100 W of power for sputtering of the corresponding metal target at a different deposition rate (Cu: 4.8 nm/min, Cr: 5 nm/min).

### 3.3. Sample preparation

The terephthalic acid solution (THA) was prepared by adding 332.4 mg of pphthalic acid and 760 mg of sodium phosphate tribasic dodecahydrate, followed by magnetic stirring for 6 h. The nitrotetrazolium blue chloride solution (NBT) was prepared by adding 10 mg to 1 liter of deionized water, followed by magnetic stirring for 6 h. A total size of 2*5 $cm^2$ of catalysts was added to a beaker containing 10 ml

of as-prepared aqueous THA (Same condition for NBT) solution, which was subsequently placed in an ultrasonic bath (40 kHz, 200 W). The catalysts were cut into a number of around 5*5 $mm^2$ pieces to improve the contact area and controllability with the aqueous solution. Aliquots were extracted at 0, 1, 2, 3, 4 h for subsequent fluorescence (UV-Vis spectrophotometry for NBT) analysis. The UV-Vis measurements for the MO samples were performed in the aforementioned sample preparation method. The temperature in the ultrasonic bath was regulated.

A 5-ppm aqueous solution of methyl orange (MO) was prepared by adding 5 mg of $C_{14}H_{14}N_3NaO_3S$ to 1 liter of deionized water, followed by magnetic stirring for 2 h.

Samples for EPR measurements were obtained by adding the same amount of catalysts to a beaker containing 10 ml of deionized water in an ultrasonication bath. About 0.1 ml of DMPO or TEMP was pipetted into the solution prior to ultrasonication.

### 3.4. Sample characterization

The charge transfer amounts were measured by electrometer (Keithley, 6514), and 200 μL of DI water per measurement. The UV-Vis spectroscopy of the aliquots was measured using a Hitachi UV-4150 UV-Visible spectrometer on a range of 200–700 nm. The emission spectra of THA–OH were measured on an Edinburgh Instruments (FLS 980), using $\lambda_{excitation}$= 312 nm and $\lambda_{emission}$= 426 nm. Electron paramagnetic resonance (EPR) was recorded on a Bruker EMX plus-9.5/12/P/L. The measurements were con ducted in X-Band (9.830243 GHz), with amplitude modulation of 1 G, microwave power of 2 mW, an amplitude modulation frequency of 100 kHz and conversion time of 60 ms, and a time constant at 40.96 ms. The Scanning electron microscopy (SEM) images of the samples were obtained using an FEI Nova 450. The Energy Dispersive X-Ray analysis (EDX) was conducted on FEI Nova 450 equipped with an AMETEK Octane Super appendix. XRD patterns of FEP/Multilayer metal composite catalysts were acquired through an advance diffractometer (Bruker-D8, Germany) with a working voltage of 40 kV. Characterization of the surface chemical state of FEP/Multilayer metal composite catalysts before and after the reaction was carried out by using X-ray photoelectron spectroscopy (XPS) on a Thermo Fisher Scientific K-Alpha. An alpha source (hv= 1486.6 eV) was used in a vacuum of $10^{-9}$ mBar with an operating voltage of 15 kV and a filament current of 10 mA. The pass energy was set to 30 eV. Metal sputtering thickness and surface roughness were observed by a step profiler (DektakXT). The scanning speed was set to 50 μm $s^{-1}$, the scanning length was 1000 μm, and the stylus force was 3 mg. Ultraviolet Photoelectron Spectroscopy (UPS) measurements were performed using the Thermo Fisher Scientific ESCALAB XI+ system. The analyzer was operated in Constant Analyzer Energy (CAE) mode with a pass energy of 1.0 eV. The lens mode was set for UPS with an energy step size of 0.05 eV and an energy step number of 601.

## Author contributions

D. Wei and Z. L. Wang proposed the idea and the project. D. Wei designed all the experiments and supervised the whole project. J. J. Liu carried out the experiments in this paper and analyzed the corresponding data. J. J. Liu and S. X. Li analyzed the operation principle of the CEC. H. Qian and T. Gan did the experiment of methanol to formaldehyde. Z. Yang and N. Wu performed DFT simulations. All the authors discussed the results and commented on the manuscript. D. Wei and J. J. Liu wrote this paper.

## CRediT authorship contribution statement

**Zhong Lin Wang:** Conceptualization. **Ning Wu:** Software. **Ting Gan:** Formal analysis. **Han Qian:** Formal analysis. **Shaoxin Li:** Writing – review & editing. **Zhe Yang:** Software. **Jiajin Liu:** Writing – review & editing, Writing – original draft, Methodology. **Di Wei:** Writing – review & editing, Conceptualization.

## Funding

This work was supported by the National Natural Science Foundation (grant number 22479016) and Beijing Natural Science Foundation (grant number 24ISB012).

## Declaration of Competing Interest

The authors declare the following financial interests/personal relationships which may be considered as potential competing interests: Di Wei reports financial support was provided by The Natural Science Foundation. Zhe Yang reports financial support was Beijing Natural Science Foundation. If there are other authors, they declare that they have no known competing financial interests or personal relationships that could have appeared to influence the work reported in this paper.

## Acknowledgements

The authors declare no competing financial interest.

## Appendix A. Supporting information

Supplementary data associated with this article can be found in the online version at doi:10.1016/j.nanoen.2025.111389.

## Data Availability

Data will be made available on request. The authors declare that all the data that support the findings of this study are available within the article and Supporting Information. Source data are provided in this paper. Correspondence and requests for materials should be addressed to D.W.

## References

[1] I. Pálinkó, Chapter 3.12 - Heterogeneous Catalysis: A Fundamental Pillar of Sustainable Synthesis, in: B. Török, T. Dransfield (Eds.), Green chemistry, Elsevier, 2018, pp. 415–447.
[2] Z. Li, S. Ji, Y. Liu, X. Cao, S. Tian, Y. Chen, Z. Niu, Y. Li, Well-Defined materials for heterogeneous catalysis: from nanoparticles to isolated SIngle-atom sites, Chem. Rev. 120 (2020) 623–682, https://doi.org/10.1021/acs.chemrev.9b00311.
[3] M. Wang, L. Li, M. Wang, X. Huang, Recent progress in palladium-nonmetal nanostructure development for fuel cell applications, NPG Asia Mater. 14 (2022) 78, https://doi.org/10.1038/s41427-022-00423-2.
[4] K. Zeng, D. Zhang, Recent progress in alkaline water electrolysis for hydrogen production and applications, Prog. Energy Combust. Sci. 36 (2010) 307–326, https://doi.org/10.1016/j.pecs.2009.11.002.
[5] R. Cao, J.-S. Lee, M. Liu, J. Cho, Recent progress in Non-Precious catalysts for Metal-Air batteries, Adv. Energy Mater. 2 (2012) 816–829, https://doi.org/10.1002/aenm.201200013.
[6] H. Dai, Environmental catalysis: a solution for the removal of atmospheric pollutants, Sci. Bull. 60 (2015) 1708–1710, https://doi.org/10.1007/s11434-015-0887-8.
[7] F. Zhan, L. Huang, Y. Luo, M. Chen, R. Tan, X. Liu, G. Liu, Z. Feng, Recent advances on support materials for enhanced Pt-based catalysts: applications in oxygen reduction reactions for electrochemical energy storage, J. Mater. Sci. (2025), https://doi.org/10.1007/s10853-025-10606-1.
[8] L. Zhang, Q. Chang, H. Chen, M. Shao, Recent advances in palladium-based electrocatalysts for fuel cell reactions and hydrogen evolution reaction, Nano Energy 29 (2016) 198–219, https://doi.org/10.1016/j.nanoen.2016.02.044.
[9] H. Lee, J.Y. Kim, S.Y. Lee, J.A. Hong, N. Kim, J. Baik, Y.J. Hwang, Comparative study of catalytic activities among transition metal-doped IrO2 nanoparticles, Sci. Rep. 8 (2018) 16777, https://doi.org/10.1038/s41598-018-35116-w.
[10] J. Tang, D. Guan, H. Xu, L. Zhao, U. Arshad, Z. Fang, T. Zhu, M. Kim, C.-W. Pao, Z. Hu, J. Ge, Z. Shao, Undoped ruthenium oxide as a stable catalyst for the acidic oxygen evolution reaction, Nat. Commun. 16 (2025) 801, https://doi.org/10.1038/s41467-025-56188-z.
[11] X. Cui, W. Li, P. Ryabchuk, K. Junge, M. Beller, Bridging homogeneous and heterogeneous catalysis by heterogeneous single-metal-site catalysts, Nat. Catal. 1 (2018) 385–397, https://doi.org/10.1038/s41929-018-0090-9.
[12] G. Gao, G. Zhao, G. Zhu, B. Sun, Z. Sun, S. Li, Y.-Q. Lan, Recent advancements in noble-metal electrocatalysts for alkaline hydrogen evolution reaction, Chin. Chem. Lett. 36 (2025) 109557, https://doi.org/10.1016/j.cclet.2024.109557.

[13] M. Borghei, J. Lehtonen, L. Liu, O.J. Rojas, Advanced Biomass-Derived electrocatalysts for the oxygen reduction reaction, Adv. Mater. 30 (2018) 1703691, https://doi.org/10.1002/adma.201703691.
[14] H. Wu, C. Feng, L. Zhang, J. Zhang, D.P. Wilkinson, Non-noble metal electrocatalysts for the hydrogen evolution reaction in water electrolysis, Electrochem. Energy Rev. 4 (2021) 473–507, https://doi.org/10.1007/s41918-020-00086-z.
[15] F. Zaera, New challenges in heterogeneous catalysis for the 21st century, Catal. Lett. 142 (2012) 501–516, https://doi.org/10.1007/s10562-012-0801-9.
[16] L. Dai, Functionalization of graphene for efficient energy conversion and storage, Acc. Chem. Res. 46 (2013) 31–42, https://doi.org/10.1021/ar300122m.
[17] M. Monai, M. Melchionna, P. Fornasiero, Chapter one - from metal to metal-free catalysts: routes to sustainable chemistry, in: C. Song (Ed.), Advances in Catalysis, Academic Press, 2018, pp. 1–73.
[18] Z. Wang, A. Berbille, Y. Feng, S. Li, L. Zhu, W. Tang, Z.L. Wang, Contact-electro-catalysis for the degradation of organic pollutants using pristine dielectric powders, Nat. Commun. 13 (2022) 130, https://doi.org/10.1038/s41467-021-27789-1.
[19] Z.L. Wang, A.C. Wang, On the origin of contact-electrification, Mater. Today 30 (2019) 34–51, https://doi.org/10.1016/j.mattod.2019.05.016.
[20] B. Baytekin, H.T. Baytekin, B.A. Grzybowski, What really drives chemical reactions on contact charged surfaces? J. Am. Chem. Soc. 134 (2012) 7223–7226, https://doi.org/10.1021/ja300925h.
[21] Y. Wei, X. Li, Z. Yang, J. Shao, Z.L. Wang, D. Wei, Contact electrification at the solid–liquid transition interface, Mater. Today 74 (2024) 2–11, https://doi.org/10.1016/j.mattod.2024.03.013.
[22] W. Dai, K. Wan, K. Pang, J. Guo, S. Liu, K. Wu, C. Tang, Y. Sun, X. Shi, Z. Tang, C. Long, F. Dong, In-depth understanding and precise modulation of surface reconstruction during heterogeneous electrocatalysis: from model to practical catalyst, Chem 11 (2025) 102345, https://doi.org/10.1016/j.chempr.2024.10.012.
[23] T. Li, O. Kasian, S. Cherevko, S. Zhang, S. Geiger, C. Scheu, P. Felfer, D. Raabe, B. Gault, K.J.J. Mayrhofer, Atomic-scale insights into surface species of electrocatalysts in three dimensions, Nat. Catal. 1 (2018) 300–305, https://doi.org/10.1038/s41929-018-0043-3.
[24] Z. Wang, X. Dong, X.-F. Li, Y. Feng, S. Li, W. Tang, Z.L. Wang, A contact-electro-catalysis process for producing reactive oxygen species by ball milling of triboelectric materials, Nat. Commun. 15 (2024) 757, https://doi.org/10.1038/s41467-024-45041-4.
[25] H.T. Baytekin, B. Baytekin, J.T. Incorvati, B.A. Grzybowski, Material transfer and polarity reversal in contact charging, Angew. Chem. Int. Ed. 51 (2012) 4843–4847, https://doi.org/10.1002/anie.201200057.
[26] J. Liu, Z. Yang, S. Li, Y. Du, Z. Zhang, J. Shao, M. Willatzen, Z.L. Wang, D. Wei, Nonaqueous contact-electro-chemistry via triboelectric charge, J. Am. Chem. Soc. 146 (2024) 31574–31584, https://doi.org/10.1021/jacs.4c09318.
[27] J. Zhao, X. Zhang, J. Xu, W. Tang, Z. Lin Wang, F. Ru Fan, Contact-electro-catalysis for direct synthesis of $H_2O_2$ under ambient conditions, Angew. Chem. Int. Ed. 62 (2023) e202300604, https://doi.org/10.1002/anie.202300604.
[28] C. Xu, S. Li, Z. Yang, M. Willatzen, Z. Lin Wang, D. Wei, Contact-electro-luminescence triggered by triboelectric charge, Chem. Eng. J. 501 (2024) 157754, https://doi.org/10.1016/j.cej.2024.157754.
[29] H. Li, A. Berbille, X. Zhao, Z. Wang, W. Tang, Z.L. Wang, A contact-electro-catalytic cathode recycling method for spent lithium-ion batteries, Nat. Energy 8 (2023) 1137–1144, https://doi.org/10.1038/s41560-023-01348-y.
[30] S. Li, Z. Zhang, P. Peng, X. Li, Z.L. Wang, D. Wei, A Green approach to induce and steer chemical reactions using inert solid dielectrics, Nano Energy 122 (2024) 109286, https://doi.org/10.1016/j.nanoen.2024.109286.
[31] X. Dong, Z. Wang, Y. Hou, Y. Feng, A. Berbille, H. Li, Z.L. Wang, W. Tang, Regulating contact-electro-catalysis using polymer/metal Janus composite catalysts, J. Am. Chem. Soc. 146 (2024) 28110–28118, https://doi.org/10.1021/jacs.4c07446.
[32] L. Pauling, The origin and nature of the electronegativity scale, J. Chem. Educ. 65 (1988) 375, https://doi.org/10.1021/ed065p375.1.
[33] X. Dong, Z. Wang, A. Berbille, X. Zhao, W. Tang, Z.L. Wang, Investigations on the contact-electro-catalysis under various ultrasonic conditions and using different electrification particles, Nano Energy 99 (2022) 107346, https://doi.org/10.1016/j.nanoen.2022.107346.
[34] L. Wang, Z. Sofer, M. Pumera, Will any crap we put into graphene increase its electrocatalytic effect? ACS Nano 14 (2020) 21–25, https://doi.org/10.1021/acsnano.9b00184.
[35] A. Martin, J. Chen, C. Du, M. Kumar, I.D. Tevis, B. Chang, S. Pathak, M.M. Thuo, Atomic reconstruction of au thin films through interfacial strains, Nano Lett. 24 (2024) 1967–1973, https://doi.org/10.1021/acs.nanolett.3c04412.
[36] I. Fridovich, The biology of oxygen radicals, Science 201 (1978) 875–880, https://doi.org/10.1126/science.210504.
[37] R.S. Sohal, R. Weindruch, Oxidative stress, caloric restriction, and aging, Science 273 (1996) 59–63, https://doi.org/10.1126/science.273.5271.59.
[38] L. Yang, R. Grzeschik, P. Jiang, L. Yu, C. Hu, A. Du, S. Schlücker, W. Xie, Tuning the electronic properties of platinum in Hybrid-Nanoparticle assemblies for use in hydrogen evolution reaction, Angew. Chem. Int. Ed. 62 (2023) e202301065, https://doi.org/10.1002/anie.202301065.
[39] A. Bzowski, T.K. Sham, Pd-Ti bimetallics: a study of the electronic structure using x-ray photoelectron spectroscopy and x-ray-absorption near-edge structure, Phys. Rev. B 48 (1993) 7836–7840, https://doi.org/10.1103/PhysRevB.48.7836.
[40] M.C. Biesinger, L.W.M. Lau, A.R. Gerson, R.S.C. Smart, Resolving surface chemical states in XPS analysis of first row transition metals, oxides and hydroxides: sc, ti, V, cu and zn, Appl. Surf. Sci. 257 (2010) 887–898, https://doi.org/10.1016/j.apsusc.2010.07.086.
[41] M.C. Biesinger, B.P. Payne, A.P. Grosvenor, L.W.M. Lau, A.R. Gerson, R.S.C. Smart, Resolving surface chemical states in XPS analysis of first row transition metals, oxides and hydroxides: cr, mn, fe, co and ni, Appl. Surf. Sci. 257 (2011) 2717–2730, https://doi.org/10.1016/j.apsusc.2010.10.051.
[42] H.-Y. Xu, B. Li, T.-N. Shi, Y. Wang, S. Komarneni, Nanoparticles of magnetite anchored onto few-layer graphene: a highly efficient Fenton-like nanocomposite catalyst, J. Colloid Interface Sci. 532 (2018) 161–170, https://doi.org/10.1016/j.jcis.2018.07.128.
[43] Y. Du, S. Fu, C. Shan, H. Wu, W. He, J. Wang, H. Guo, G. Li, Z. Wang, C. Hu, A novel design based on mechanical time-delay switch and charge space accumulation for high output performance direct-current triboelectric nanogenerator, Adv. Funct. Mater. 32 (2022) 2208783, https://doi.org/10.1002/adfm.202208783.
[44] S. Li, Z. Zhang, F. Yang, X. Li, P. Peng, Y. Du, Q. Zeng, M. Willatzen, Z.L. Wang, D. Wei, Transistor-like triboiontronics with record-high charge density for self-powered sensors and neurologic analogs, Device (2024) 100332, https://doi.org/10.1016/j.device.2024.100332.
[45] Y. Nosaka, A.Y. Nosaka, Generation and detection of reactive oxygen species in photocatalysis, Chem. Rev. 117 (2017) 11302–11336, https://doi.org/10.1021/acs.chemrev.7b00161.
[46] X.-F. Li, A. Berbille, T.-Y. Wang, X. Zhao, S. Li, Y. Su, H. Li, G. Zhang, Z. Wang, L. Zhu, J. Liu, Z.L. Wang, Defect passivation toward designing High-Performance fluorinated polymers for Liquid–Solid Contact-Electrification and Contact-Electro-Catalysis, Adv. Funct. Mater. 34 (2024) 2315817, https://doi.org/10.1002/adfm.202315817.
[47] Y. Su, A. Berbille, Z.L. Wang, W. Tang, Water-solid contact electrification and catalysis adjusted by surface functional groups, Nano Res. 17 (2024) 3344–3351, https://doi.org/10.1007/s12274-023-6125-9.
[48] X. Zhao, Y. Su, A. Berbille, Z.L. Wang, W. Tang, Degradation of methyl Orange by dielectric films based on contact-electro-catalysis, Nanoscale 15 (2023) 6243–6251, https://doi.org/10.1039/D2NR06783H.
[49] L.E. Heim, H. Konnerth, M.H.G. Prechtl, Future perspectives for formaldehyde: pathways for reductive synthesis and energy storage, Green. Chem. 19 (2017) 2347–2355, https://doi.org/10.1039/C6GC03093A.
[50] T. Cai, H. Sun, J. Qiao, L. Zhu, F. Zhang, J. Zhang, Z. Tang, X. Wei, J. Yang, Q. Yuan, W. Wang, X. Yang, H. Chu, Q. Wang, C. You, H. Ma, Y. Sun, Y. Li, C. Li, H. Jiang, Q. Wang, Y. Ma, Cell-free chemoenzymatic starch synthesis from carbon dioxide, Science 373 (2021) 1523–1527, https://doi.org/10.1126/science.abh4049.
[51] R.G. Herman, Q. Sun, C. Shi, K. Klier, C.-B. Wang, H. Hu, I.E. Wachs, M.M. Bhasin, Development of active oxide catalysts for the direct oxidation of methane to formaldehyde, Catal. Today 37 (1997) 1–14, https://doi.org/10.1016/S0920-5861(96)00256-8.
[52] K. Wachi, T. Yabe, T. Suzuki, K. Yonesato, K. Suzuki, K. Yamaguchi, Role of polyoxometalate precursors and supports in the selective oxidation of methane into formaldehyde using supported metal oxide subnanocluster catalysts, Catal. Sci. Technol. 13 (2023) 4744–4752, https://doi.org/10.1039/D3CY00750B.
[53] J. Bin Yeo, J. Ho Jang, Y. In Jo, J. Woo Koo, K. Tae Nam, Paired electrosynthesis of formaldehyde derivatives from $CO_2$ reduction and methanol oxidation, Angew. Chem. Int. Ed. 63 (2024) e202316020, https://doi.org/10.1002/anie.202316020.
[54] J. Chen, S. Stepanovic, A. Draksharapu, M. Gruden, W.R. Browne, A Non-Heme iron photocatalyst for Light-Driven aerobic oxidation of methanol, Angew. Chem. Int. Ed. 57 (2018) 3207–3211, https://doi.org/10.1002/anie.201712678.
[55] R. Zhang, J. Shi, L. Fu, Y.-G. Liu, Y. Jia, Z. Han, K. Yuan, H.-Y. Jiang, Direct photocatalytic methane oxidation to formaldehyde by n doping Co-decorated mixed crystal $TiO_2$, ACS Nano 18 (2024) 12994–13005, https://doi.org/10.1021/acsnano.4c01318.
[56] W. Li, J. Sun, M. Wang, J. Xu, Y. Wang, L. Yang, R. Yan, H. He, S. Wang, W.-Q. Deng, Z.-Q. Tian, F.R. Fan, Contact-electro-catalysis for direct oxidation of methane under ambient conditions, Angew. Chem. Int. Ed. 63 (2024) e202403114, https://doi.org/10.1002/anie.202403114.